U.S. DEPARTMENT OF COMMERCE
National Technical Information Service

AD-A027 209

10.6 MICROMETER COHERENT MONOPULSE TRACKING INTERIM RESULTS

MASSACHUSETTS INSTITUTE OF TECHNOLOGY

PREPARED FOR
ELECTRONIC SYSTEMS DIVISION

7 MAY 1976

BEST
AVAILABLE COPY

MISSING PAGE
NUMBERS ARE BLANK
AND WERE NOT
FILMED

209051

Technical Note

1976-19

R. Teoste
W. J. Scouler

10.6 μm Coherent Monopulse Tracking Interim Results

7 May 1976

Prepared for the Defense Advanced Research Projects Agency
under Electronic Systems Division Contract F19628-76-C-0002 by

Lincoln Laboratory
MASSACHUSETTS INSTITUTE OF TECHNOLOGY
LEXINGTON, MASSACHUSETTS

Approved for public release; distribution unlimited.

NATIONAL TECHNICAL
INFORMATION SERVICE

AD A027209

The work reported in this document was performed at Lincoln Laboratory, a center for research operated by Massachusetts Institute of Technology. This work was sponsored by the Defense Advanced Research Projects Agency under Air Force Contract F19628-76-C-0002 (ARPA Order 600).

This report may be reproduced to satisfy needs of U.S. Government agencies.

The views and conclusions contained in this document are those of the contractor and should not be interpreted as necessarily representing the official policies, either expressed or implied, of the Defense Advanced Research Projects Agency of the United States Government.

This technical report has been reviewed and is approved for publication.

FOR THE COMMANDER

William H. Lawton

William H. Lawton, Lt. Col., USAF
Acting Chief, ESD Lincoln Laboratory Project Office

REPORT DOCUMENTATION PAGE		READ INSTRUCTIONS BEFORE COMPLETING FORM
1. REPORT NUMBER ESD-TR-76-107	2. GOVT ACCESSION NO.	3. RECIPIENT'S CATALOG NUMBER
4. TITLE (and Subtitle) 10.6 μm Coherent Monopulse Tracking Interim Results		5. TYPE OF REPORT & PERIOD COVERED Technical Note 6. PERFORMING ORG. REPORT NUMBER Technical Note 1976-19
7. AUTHOR(s) Rein Teoste William J. Scouler		8. CONTRACT OR GRANT NUMBER(s) F19628-76-C-0002
9. PERFORMING ORGANIZATION NAME AND ADDRESS Lincoln Laboratory, M.I.T. P.O. Box 73 Lexington, MA 02173		10. PROGRAM ELEMENT, PROJECT, TASK AREA & WORK UNIT NUMBERS ARPA Order 600 Program Element No. 62301E Project No. 6E20
11. CONTROLLING OFFICE NAME AND ADDRESS Defense Advanced Research Projects Agency 1400 Wilson Boulevard Arlington, VA 22209		12. REPORT DATE 7 May 1976 13. NUMBER OF PAGES 48
14. MONITORING AGENCY NAME & ADDRESS (if different from Controlling Office) Electronic Systems Division Hanscom AFB Bedford, MA 01731		15. SECURITY CLASS. (of this report) Unclassified 15a. DECLASSIFICATION DOWNGRADING SCHEDULE
16. DISTRIBUTION STATEMENT (of this Report) Approved for public release; distribution unlimited.		
17. DISTRIBUTION STATEMENT (of the abstract entered in Block 20, if different from Report)		
18. SUPPLEMENTARY NOTES None		
19. KEY WORDS (Continue on reverse side if necessary and identify by block number) monopulse tracking IR radar satellite tracking atmospheric turbulence effects GEOS-III satellite retroreflector		

20. ABSTRACT (Continue on reverse side if necessary and identify by block number)

This report describes the present status and recent results of 10.6 μm monopulse radar tracking experiments. Included is a description of the radar system and results of short range (<20 km) and long range (>150 km) tracking experiments which show that useful monopulse processing of IR radar returns can be accomplished. The short range experiments involved a stationary test tower and a moving cooperative aircraft. The long range experiment demonstrated, for the first time, 10.6 μm coherent monopulse tracking of a satellite.

PRICES SUBJECT TO CHANGE

DD FORM 1 JAN 73 1473 EDITION OF 1 NOV 65 IS OBSOLETE

MASSACHUSETTS INSTITUTE OF TECHNOLOGY
LINCOLN LABORATORY

10.6 μm COHERENT MONOPULSE TRACKING INTERIM RESULTS

R. TEOSTE
W. J. SCOULER
Group 54

TECHNICAL NOTE 1976-19

7 MAY 1976

Approved for public release; distribution unlimited.

LEXINGTON MASSACHUSETTS

11 a-

ABSTRACT

This report describes the present status and recent results of 10.6 μm monopulse radar tracking experiments. Included is a description of the radar system and results of short range (<20 km) and long range (>150 km) tracking experiments which show that useful monopulse processing of IR radar returns can be accomplished. The short range experiments involved a stationary test tower and a moving cooperative aircraft. The long range experiment demonstrated, for the first time, 10.6 μm coherent monopulse tracking of a satellite.

Preceding page blank

CONTENTS

Preceding page blank

LIST OF FIGURES

I. INTRODUCTION

This report describes the present status and recent results of 10.6 μm monopulse radar tracking experiments at the Firepond IR Radar Facility. Included is a description of the radar system and results of short range (<20 km) and long range (>150 km) tracking experiments which show that useful monopulse processing of IR radar returns can be accomplished. The short range experiments involved testing of the system and measurement of atmospheric turbulence effects on a stationary test tower as well as tracking a moving cooperative aircraft. The long range experiment demonstrated, for the first time, 10.6 μm coherent monopulse tracking of the GEOS-III geodetic satellite equipped with a retroreflector. The RMS tracking precision was 1 μrad.

II. SYSTEM DESCRIPTION

A. Introduction

The infrared radar subsystems relevant for tracking are shown in Figure 1. A single frequency master oscillator (MO) generates a stable frequency IR beam which is amplified and then modulated by slots in a mechanically rotated chopper disk. The beam is directed by mirrors and lenses to the 1.2 meter azimuth/elevation telescope system which points the beam toward the desired target. A servo controlled vernier mirror can be used to make small corrections in the radar line-of-sight pointing. Transmitted and reflected energy to and from the target travel through the atmosphere and are received through the same optical system. The modulating chopper disc also serves as a duplexer and reflects the returned beam onto the detector, where it is mixed with the local oscillator (LO) signal and

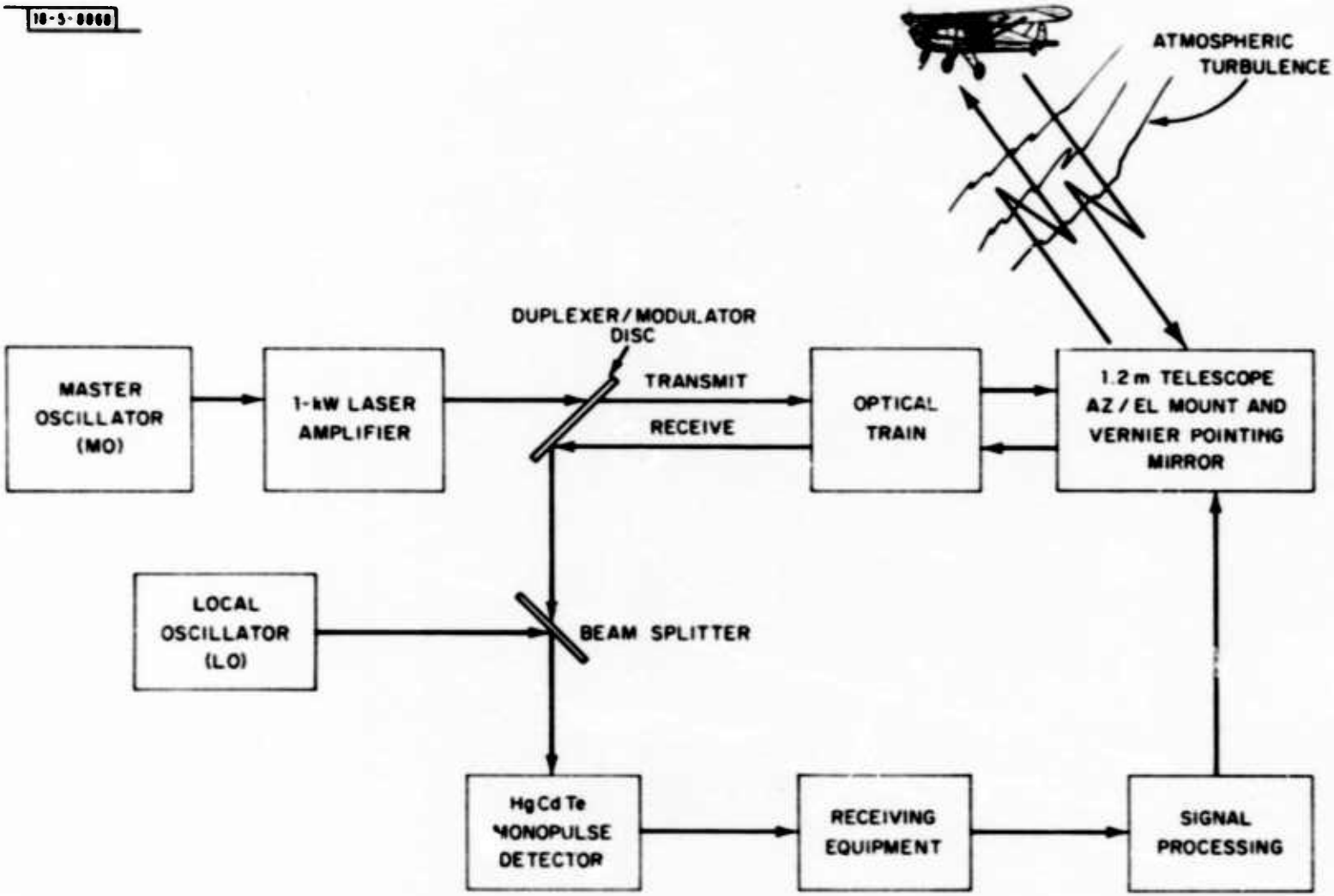

Fig. 1. Coherent IR monopulse tracking radar system.

coherently detected. The signals are coherently processed by the receiving equipment to produce azimuth and elevation pointing control information.

While the block diagram of the IR radar resembles that of a microwave radar, the shorter wavelength produces some unique characteristics, as summarized by Table 1. In particular, the transmit/receive beamwidth of 10 μrad is two to three orders of magnitude narrower than that attained by typical large microwave radar dishes. This narrow beamwidth allows very accurate angle tracking, which is described in this report.

B. EQUIPMENT

1. Telescope

Figure 2 depicts a cut-away view of the telescope and main laboratory area. The 1.2 m diameter elevation-over-azimuth telescope, which is used to both transmit and receive the 10.6 μm radiation, is housed in a dome about 10 m from the ground. This telescope produces a diffraction-limited beam with a half-power angular spread of about 10 μrad at 10.6 μm. A servo controlled vernier mirror (scanner) for fine pointing and corrections to the main mount is located on the elevation axis.

The optical path from the scanner to the main laboratory area is enclosed in tubing in which a high-velocity (~10 m/sec) filtered air flow is maintained in order to produce a clean, uniform, optical medium. Also included in this path is an aerodynamic mixing section near the main laboratory end of the path which reduces optical distortions due to temperature differences in the air path between the main laboratory and

TABLE 1

FIREPOND IR RADAR CHARACTERISTICS

Parameter	Short Range Mode	Long Range Mode
Operating Wavelength	10.6 μm	10.6 μm
Waveform	10 μsec	1, 2, 4 ms pulse
Typical Transmitted Peak Power	10-100 μW	400 W
Pulse Repetition Frequency	4750/second	250, 125, 62.5/sec
Duty Cycle	.05	.25
Minimum Detectable Power	$\sim 10^{-19}$ W/Hz	$\sim 10^{-19}$ W/Hz
3 dB Beamwidth	10 μrad	10 μrad
Typical Operating Range	5-20 km	1000 km
Typical Doppler Shift	0-2 MHz	0-1200 MHz
Target	3 cm retroreflector	3.8 cm retroreflector

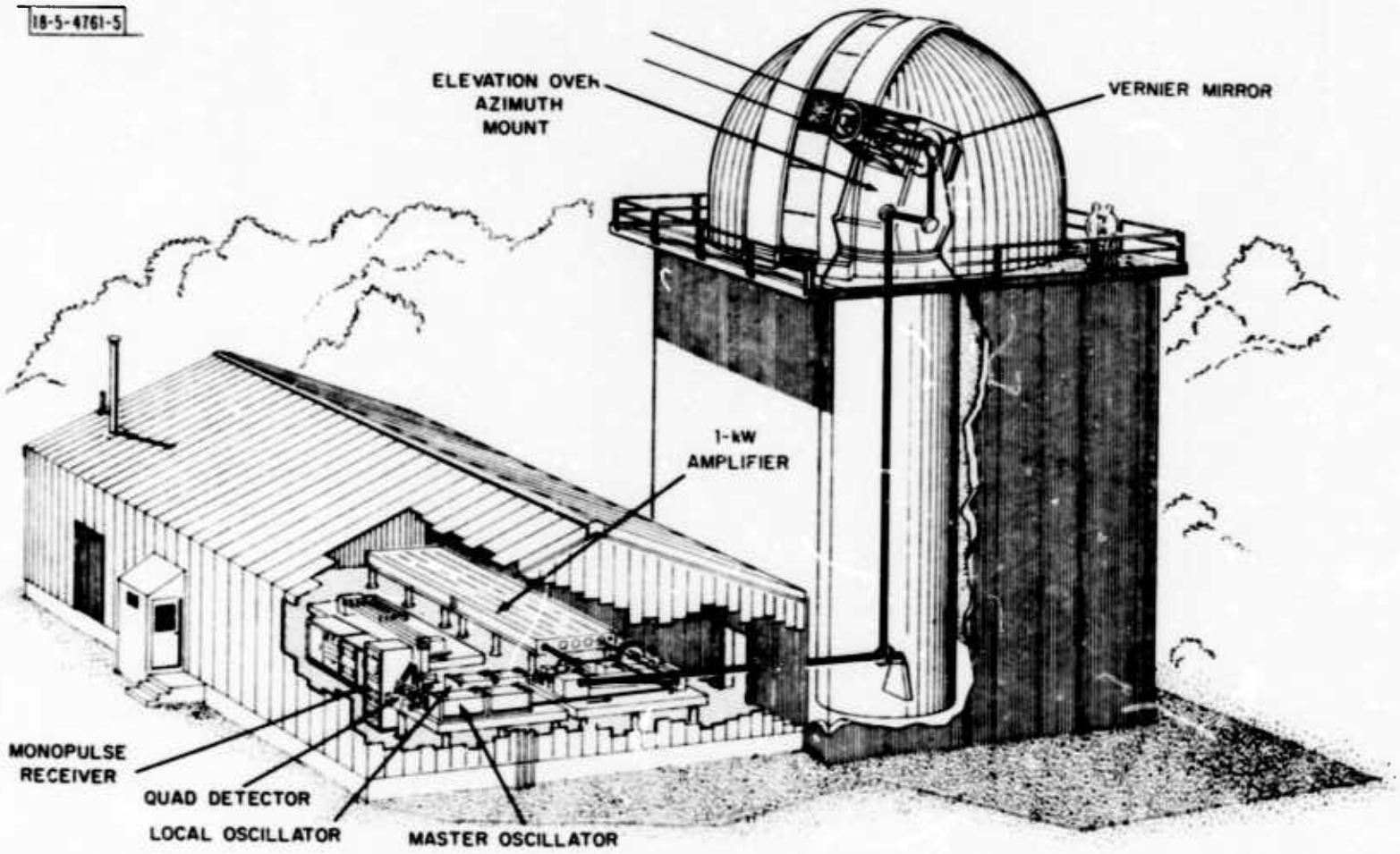

Fig. 2. IR radar system layout.

the tower. Enclosed in the tubing are fold mirrors which direct the transmit and receive beams between the laboratory area and the telescope.

2. Transmitter

The laboratory area transmit and receive system is depicted in more detail in Figure 3. The transmit beam originates in the 10.6 μm laser MO in the lower left. In order to lock the local oscillator frequency to the master oscillator frequency, a small portion of the MO beam is split off for use in a "Δf loop" which maintains a constant $f_{MO} - f_{LO}$ frequency difference. The rest of the MO beam is focused onto the plane of the duplexer disk. The duplexer is a polished mirror containing slots and holes for chopping the MO beam and producing pulses. Table 1 lists the PRF's and duty cycles currently available. The MO beam goes through a slot (or hole) in the duplexer and is then collimated and folded into the CO_2 laser amplifier which is a series of gas discharge tubes capable of amplifying a few watts of MO power to a maximum of about 1 kW peak power. A HeNe alignment laser is combined with the MO 10.6 μm beam at the 1 kW amplifier input for aligning the amplifier mirrors in the tubes by visual inspection. The output of the 1 kW amplifier is refocused and transmitted through another slot in the duplexer, folded and recollimated to a 6" beam by an off-axis paraboloid for transmission to the telescope tower. There it is expanded again 8 times by the telescope and pointed to the target.

3. Receiver Optics

Radiation scattered by a target in the path of the transmit beam is collected by the telescope and follows a path back to the duplexer identical to that of the transmit beam. However, the rotating duplexer has moved to

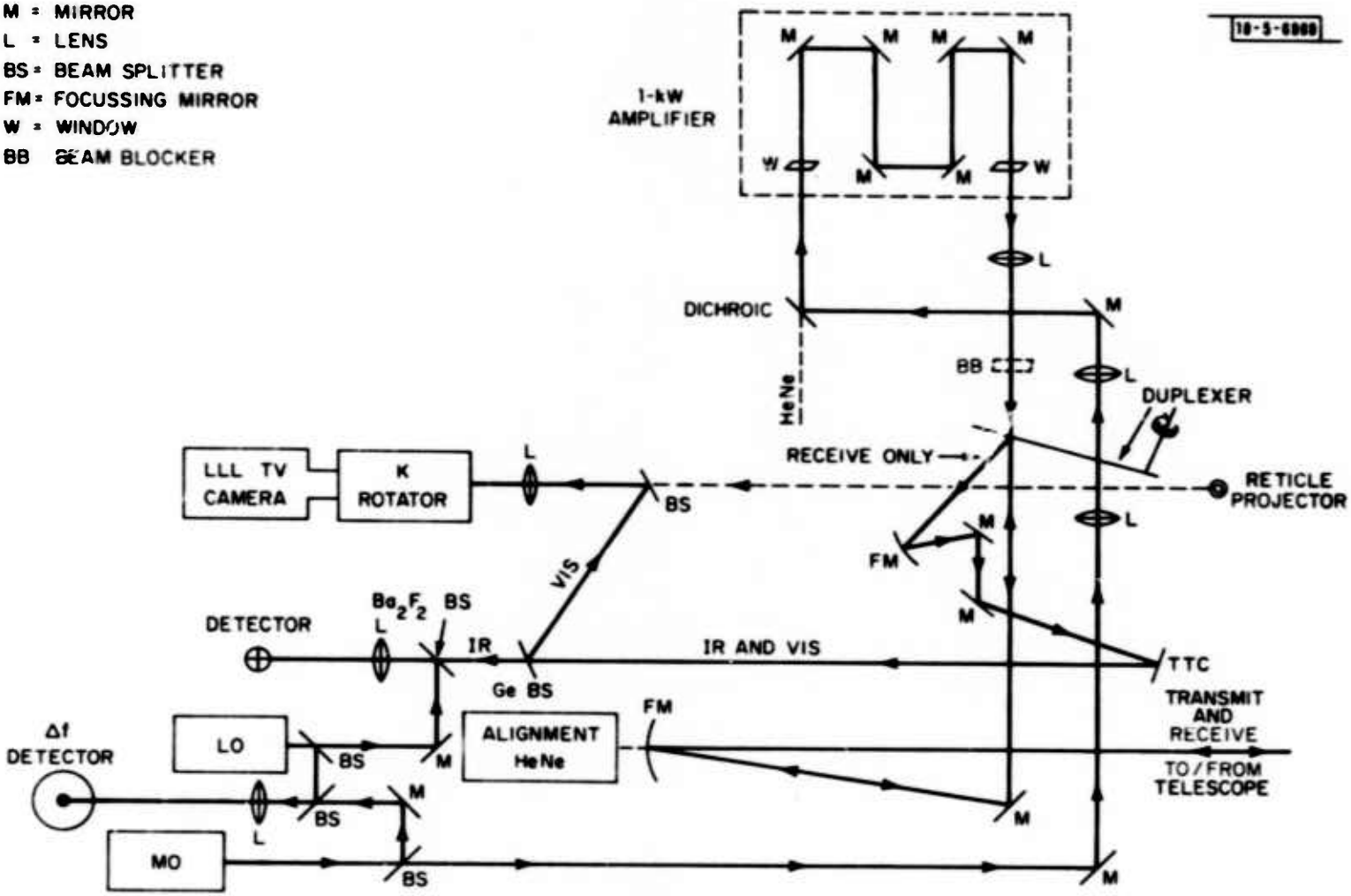

Fig. 3. Lower optical system layout.

a reflecting mode between the time of transmit and receive and the received beam now follows a path through the receiver optics as indicated by "Receive Only." The received beam, which is focused on the duplexer mirror surface, is recollimated by a small off-axis paraboloid. The 3.5 cm diameter beam is folded and then reflected by the transit time corrector (TTC). The TTC is a servo-controlled mirror which makes angle corrections to compensate for the finite transit time of the transmit and receive beams to and from a moving target (i.e., the transmit beam must point ahead of the received beam from a moving target by an amount which depends on the transverse velocity of the target).

Up to this point, the received beam contains both visible and 10.6 μm radiation. The visible radiation is typically solar illumination reflected by the target and can be used to produce a TV image for visible acquisition and tracking. Since the visible and 10.6 μm radiation are collinear except for the small difference in atmospheric refraction, the visible image is used to point the 10.6 μm beam to the target. The visible radiation is split off by a Ge beam splitter and focused onto a low light level TV (LLLTV). A "K" rotator compensates for rotation of the visible image caused by the telescope moving with respect to the receiver optics. An alignment reticle is projected through the partially transmitting mirror and also focused on the LLLTV. The reticle represents boresite and the location where 10.6 μm returns will be seen by the detector.

The coherent detection process is depicted in Figure 4 and is described in more detail in references 1 and 2. A signal beam at frequency f_S and a local oscillator beam at f_{LO} are combined at the beam splitter and focused together onto a detector which is the mixer. The detector

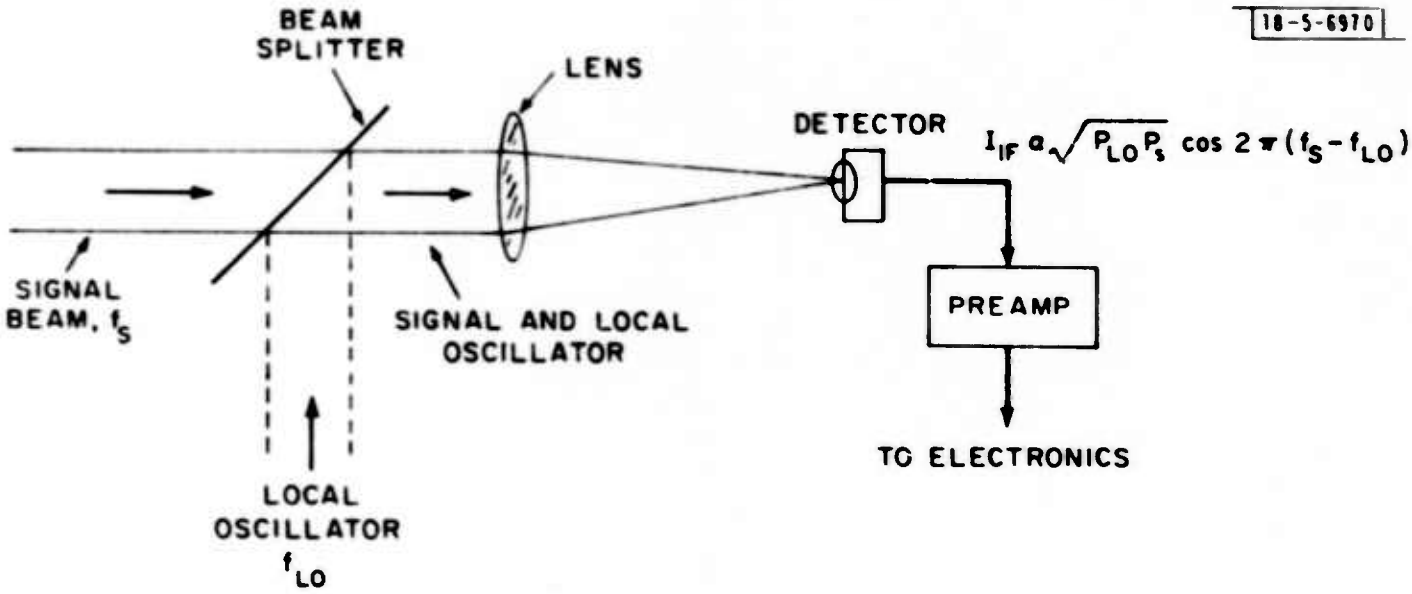

Fig. 4. Coherent detection schematic.

produces an IF signal at $f_s - f_{LO}$ whose power is proportional to the product of the signal and LO power. In our case, the received signal from a moving target is at $f_s = f_{MO} + f_D$ where f_{MO} is the master oscillator frequency and f_D the doppler shift. Therefore $f_{IF} = f_s - f_{LO} = f_{MO} + f_D - f_{LO}$. The components at the left side of Figure 3, where a portion of the MO and LO are mixed in the "Δf" detector, serve to maintain $f_{MO} - f_{LO}$ at a constant value of 10 MHz. Thus, f_{IF} is directly related to f_D and the IF signal can thus be analyzed for information about motion of the target.

4. Detector

The detector is a special HgCdTe 2 x 2 quad array especially fabricated for use in IR tracking experiments by the Solid State Division of Lincoln Laboratory. A detailed description of its characteristics is available in a report by D. L. Spears.[3] Basically, it is a 280 μm diameter array sensitive to 10.6 μm radiation and capable of producing heterodyne signals to 1200 MHz, which is the present doppler limit. (As a guide 1 m/sec radial velocity produces a 200 kHz doppler shift. Satellite tangential velocities are 8 km/sec which is greater than the 6 km/sec system capability. Thus, our system is capable of observing components of the satellite motion in the direction of the telescope up to a magnitude of 6 km/sec. This occurs typically above elevation angles of 20°.) The detector operates at 77°K. It has a minimum detectable signal power per unit bandwidth of less than 1×10^{-19} W/Hz and about 30 dB RF isolation between elements of the quad array. An optimum LO power of about 0.5 mW on each quadrant produces enough conversion gain so that the signal predominates over front end preamp noise of the receiver electronics.

The signal and LO beams are focused to give a difraction limited Airy

disk approximately equal to the detector diameter. When the signal is centered on the detector (boresight), equal signal is generated in each quadrant of the array. If the signal is off boresight due to a tracking error, unequal signals are generated in the quad elements giving rise to monopulse error signals which can be used for tracking purposes as described below.

5. Receiver Electronics

Figure 5 shows a block diagram depicting the monopulse error signal processing. The IF signals from each of the detector quadrants are processed by the monopulse receiver, the original version of which was designed and built by Airborne Instrumentation Laboratories, to produce sum, Δx and Δy signals. The additional error processor removes biases present in the receiver in addition to improving the ability to extract weak signals from noise. The coordinate converter compensates for the rotation of the image caused by the rotation of the telescope image with respect to the stationary receiver optics. The Δx and Δy error signals are thus converted to azimuth (ΔAz) and elevation (ΔEl) errors in the sky. The error signals are transmitted to the computer which then commands appropriate servo motion of the scanner or telescope to reduce the error to zero bringing the target back on boresight.

The receiver is shown in more detail in Figure 6. After amplification by the low noise preamps, the quad element IF signals are processed by a hybrid comparator yielding Δx, Δy, and Σ signals. After further amplification, these signals are mixed with the output of the computer commanded frequency tracker yielding 1560 Mhz IF signals. The frequency tracker uses target trajectory information to give an output 1560Mhz different from the expected

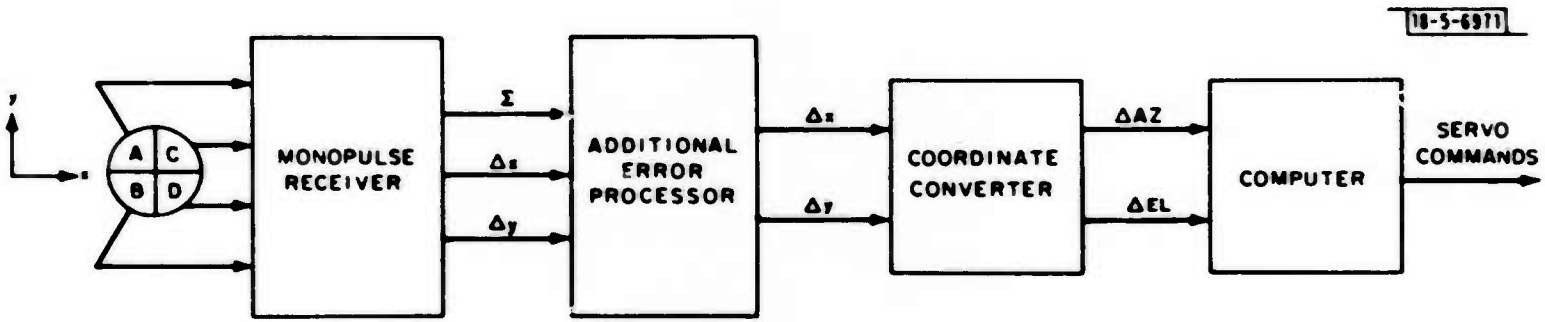

Fig. 5. Monopulse electronics block diagram.

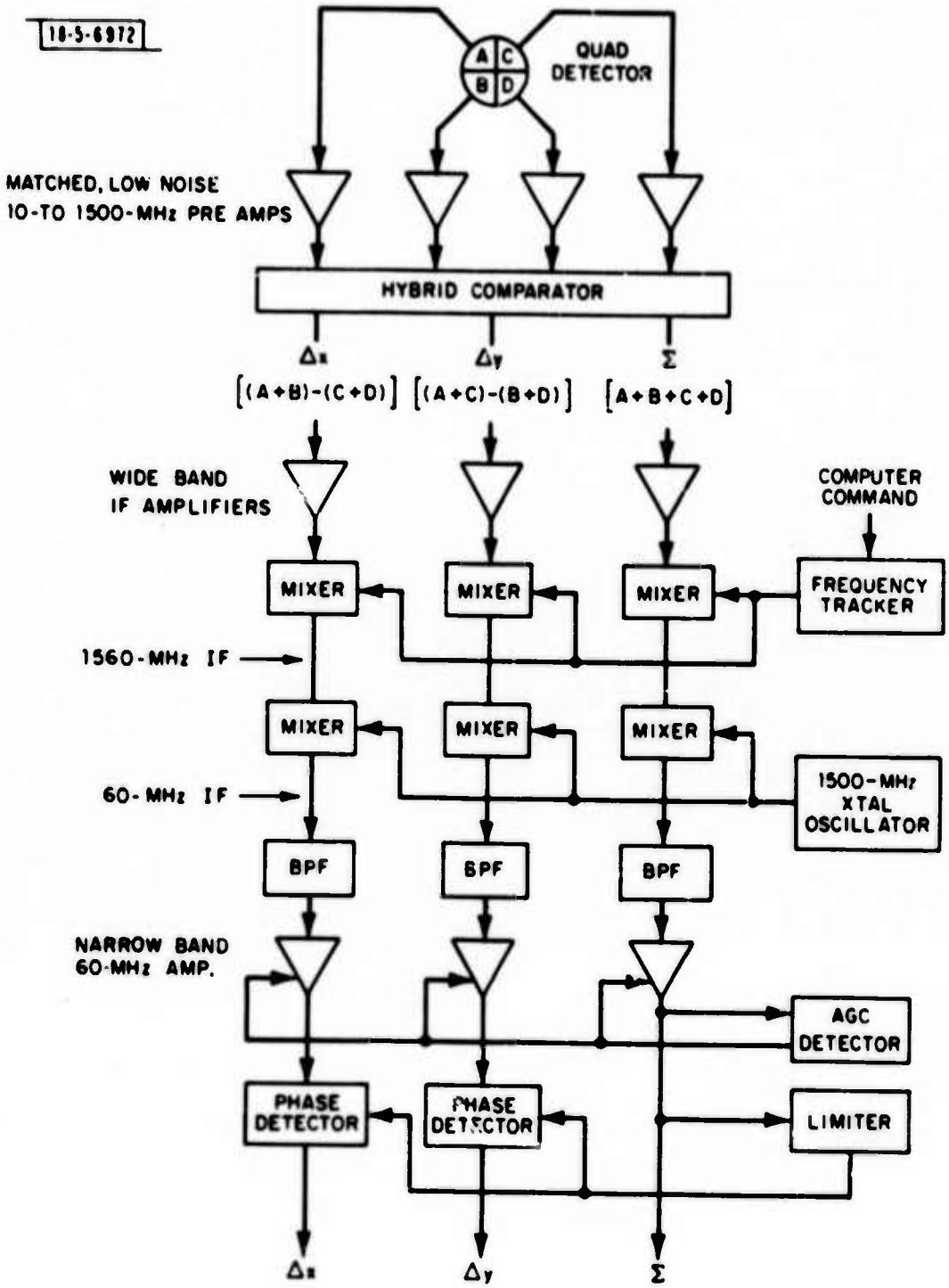

Fig. 6. Monopulse receiver.

signal frequency which may be doppler shifted due to target motion. The 1560 Mhz Δx, Δy and Σ signals are then mixed with a 1500 Mhz crystal oscillator yielding 60 Mhz signals. These are filtered and further amplified under automatic gain control (AGC). The error signals are then phase detected using the sum channel as a reference.

Because the nominal satellite range rate and therefore the doppler shift information is not accurate, the angle error determination is accomplished in a 1 Mhz bandwidth system. The doppler spread of a target is much narrower than 1 Mhz, typically less than .1 Mhz, consequently the signal-to-noise ratio of the error signals is much lower than could be obtained by optimum bandwidths.

The receiver output contains biases and does not produce useful error signals at low signal/noise ratios ($S/N << 1$). Thus, additional error processing was added which essentially "chops" the output, removes the effect of biases and permits operation with low signal levels. Two methods of processing have been developed, one for short range targets and one for long range targets.

As Figure 7 shows, the chopping in the short range mode is accomplished by producing two successive range gates of 10 μsec duration, 20 μsec apart. The first gate, during a received pulse period permits sampling of signal plus noise and biases. The second gate, permits sampling during another gate when only biases and noise are present. The two samples are subtracted in a differential amplifier and amplified yielding the net signal with residual noise. This method of additional error signal processing is termed "range gate switching". Note that no normalization is performed with the sum

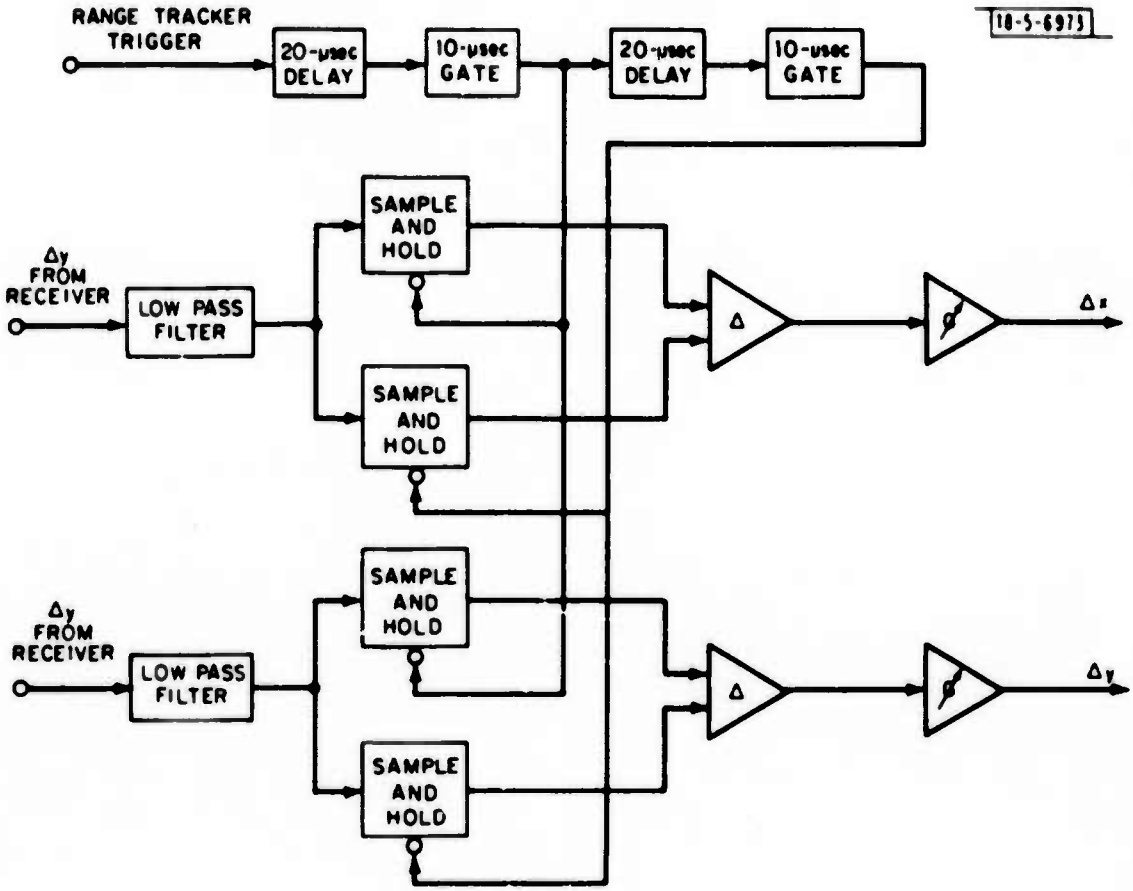

Fig. 7. Short-range error processor.

signal, since the signal strength in short pulse mode experiments has been sufficient to have an effective AGC which performs the normalization.

The second method of "chopping" used in the long range mode where a satellite may be tracked is shown in Figure 6. In this method, the computer commands the frequency tracker to switch the frequency by an amount $\pm\Delta f$ from its nominal "signal" value f on every other pulse. Thus the receiver processes pulses at f, $f + \Delta f$, f, $f - \Delta f$, f, etc. in sequence. Δf, typically 2.5 MHz, is chosen to be greater than the bandwidth of the receiver which is selectively $\pm .5$ MHz or ± 50 kHz around f. Thus, when the receiver is tuned for frequency f, the receiver processes pulses containing the signal at f yielding signal plus noise and biases. When the receiver is tuned for frequency $f \pm \Delta f$, signals at f are not processed and the receiver yields only noise and biases. These two different samples taken during successive range gates are held and subtracted in a differential amplifier, yielding the net signal and residual noise. An added feature of the long range processor is normalization which is produced by dividing the error signal by the sum signal as shown in Figure 8. This method of normalization was added because the AGC is not effective at low signal levels which is the case in the long range mode.

It is obvious that this "frequency switching" method has the disadvantage of only using half the number of useful received pulses. Every pulse potentially has a received signal in it but we only allow half of them to "get through" the receiver. In range gate switching, as in the short range mode, every pulse is used, but there an extra range gate of 10 μsec only uses up another 5% of the pulse repetition interval of 200 μsec.

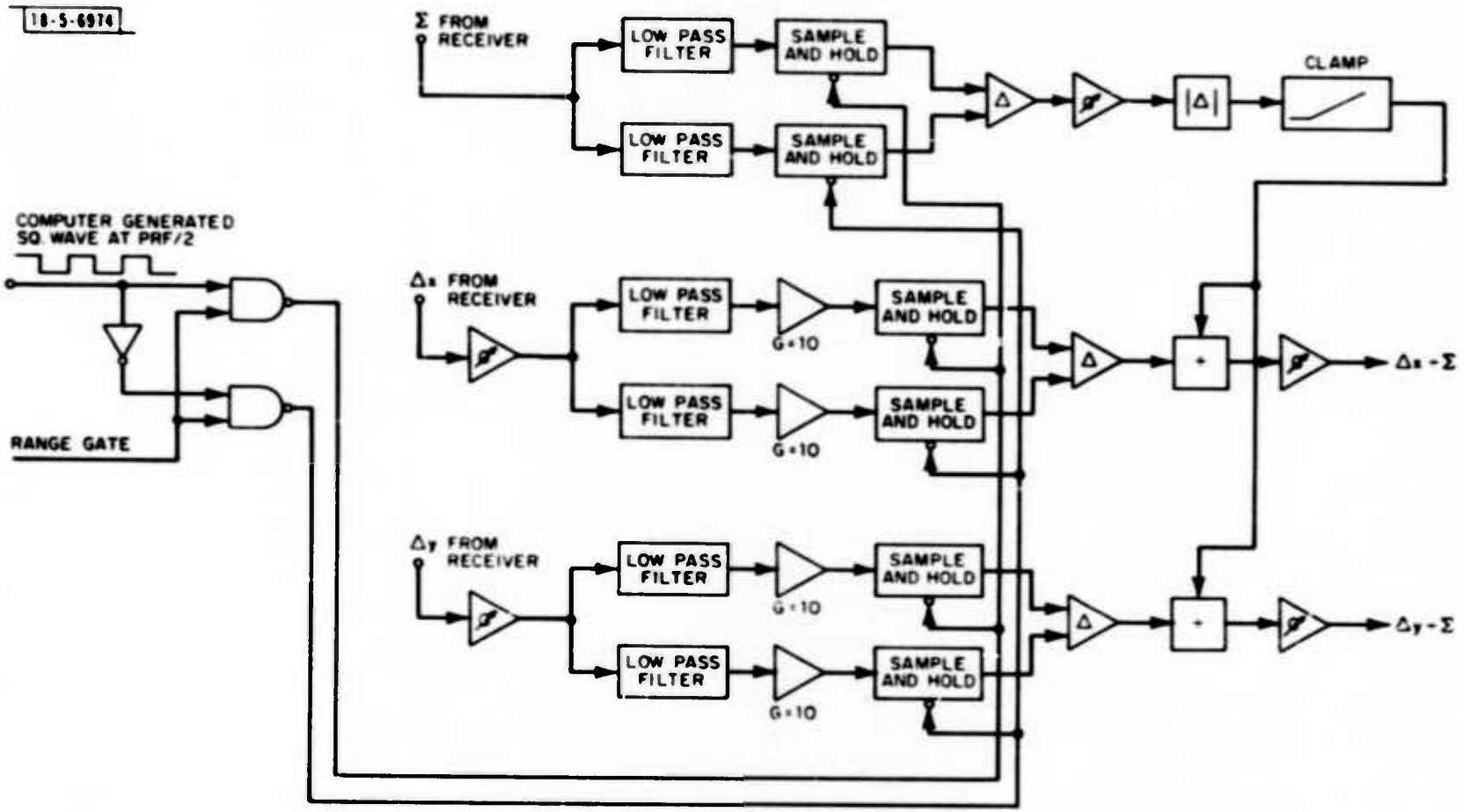

Fig. 8. Long range error processor.

In the long range mode with its 25% duty cycle, it is not convenient due to other limitations to squeeze in another gate either before or after the received pulse and thus frequency switching is used.

6. Tracking Loops

The monopulse error signals are sampled, quantized and transmitted to the computer where the tracking loops are implemented by digital filtering. The computer is a Systems Engineering Laboratories SEL 86 with a memory cycle time of 600 nsec. Filtering is performed with minimal computational time delay; however, the servo loop response is affected by the data transmission delays to and from the computer.

There are two tracking loops; the first loop is closed around the vernier mirror and the second loop around the telescope main mount. A "cascade" mode exists in the software, which allows the vernier mirror to track the target in a small field-of-view and correct the telescope mount position whenever the vernier mirror is not in its nominal zero position. The combination of these two loops allows large angle variations to be tracked out by control loops of moderate bandwidth.

a. Vernier Tracking Loop

The vernier mirror tracking loop is a simple first order loop. First and second order exponential tracking loops are used in the system which are described mathematically by Brown.[4] In this loop, the error signals ε are filtered by

$$\hat{x}(t) = \hat{x}(t - \Delta t) + K\,\varepsilon(t) \qquad (1)$$

where $\hat{x}$ is one of the estimated tracked angles (azimuth or elevation) at

time t and K is the servo gain constant which is adjusted in real time to produce a compromise of best transient response and smoothness of track. The sampling interval Δt is 20 milliseconds if monopulse error data is available. When no returns are observed the old estimate of the angle $\hat{x}$ is retained.

The computation defined by (1) produces a type I servo loop; that is, it estimates the constant value of x with no tracking error; but, has a steady state lag which is proportional to the velocity of the target. The steady state magnitude of the lag error is $(\frac{1-K}{K})\Delta t$ times the velocity of the target.

The response of the tracking loop is controlled primarily by the software filtering. The desired vernier mirror position is computed by Equation 1 and the commands are transmitted to the vernier mirror control servo. The mirror servo has finite response and the command electronics finite delays. When the servo gain K, in Equation 1, is made as large as possible, delays caused by hardware, software, and the servo response presently limit the vernier tracking loop bandwidth to about three Hz.

When the vernier mirror tracking loop is used, the telescope azimuth/elevation mount is commanded to follow the target according to best available predicted target position, e.g., microwave radar tracking data, nominal satellite trajectory information, a fixed test tower position, etc. The differences in the predicted and the observed target positions are usually small and would require modest servo response, except that atmospheric turbulence effects can be a substantial part of this difference and require

fast servo response. As we will see, severe atmospheric turublence can prevent monopulse tracking at all with the existing system.

b. Telescope Mount Tracking Loops

The three telescope mount tracking loops are aided track mode, aircraft track mode and cascade track mode.

The aided tracking loop is similar to the vernier mirror Type I tracking loop. The mount is commanded to follow the predicted target position and the monopulse tracked differences are added to the predicted target position at a sampling rate of 50/second.

In the aircraft track mode no apriori positional information is available, and the tracker must handle very large velocities. A Type I tracking loop would have lag errors much larger than a beamwidth, causing the IR monopulse system to lose track. For this reason in the aircraft tracking mode, a Type II telescope mount tracking loop is implemented which would follow a constant velocity target with no steady state errors.

We assume that the input to the filter x(t) is a linear function of time (t) as described by a and b in

$$x(t) = a + bt \tag{2}$$

and we wish to estimate a and b.

The recursive relations for the filter operators $\hat{S}^1$ and $\hat{S}^2$ are

$$\begin{bmatrix} \hat{S}^{[1]}(t) \\ \hat{S}^{[2]}(t) \end{bmatrix} = \begin{bmatrix} (1 - k) & 0 \\ k(1 - k) & (1 - k) \end{bmatrix} \begin{bmatrix} \hat{S}^{[1]}(t - \Delta t) \\ \hat{S}^{[2]}(t - \Delta t) \end{bmatrix} + \begin{bmatrix} k \\ k^2 \end{bmatrix} [x(t) - S^{[1]}(t - \Delta t)] \quad (3)$$

and the position a + th and velocity b estimates at time t are

$$\begin{bmatrix} \hat{x}(t) \\ \dot{\hat{x}}(t) \end{bmatrix} = \begin{bmatrix} \hat{a}(t) + t\,\hat{b}(t) \\ \hat{b}(t) \end{bmatrix} = \begin{bmatrix} 2 & -1 \\ \frac{k}{1 - k} & \frac{-k}{1 - k} \end{bmatrix} \begin{bmatrix} \hat{S}^{[1]}(t) \\ \hat{S}^{[2]}(t) \end{bmatrix} \quad (4)$$

where the servo gain k is adjusted for optimum performance.

For initialization of the filter

$$\begin{bmatrix} \hat{S}^{[1]}(t) \\ \hat{S}^{[2]}(t) \end{bmatrix} = \begin{bmatrix} 1 & (t - \frac{1 - k}{k}) \\ 1 & (t - \frac{2 - 2k}{k}) \end{bmatrix} \begin{bmatrix} \hat{a} \\ \hat{b} \end{bmatrix} \quad (5)$$

$S^{[1]}$ and $S^{[2]}$ are set in the system by several means; however, most commonly, b is changed by handwheels until the target position and velocity match those of the filter.

x(t) to be used in Equation 3 is derived from the monopulse errors and the telescope line-of-sight. These aircraft tracking computations are performed only 10 times a second.

The cascade aircraft tracking loop is shown in Figure 9. Here the monopulse error signals are tracked with the vernier mirror tracking loop and the main mount position tracking loop moves the telescope so that the

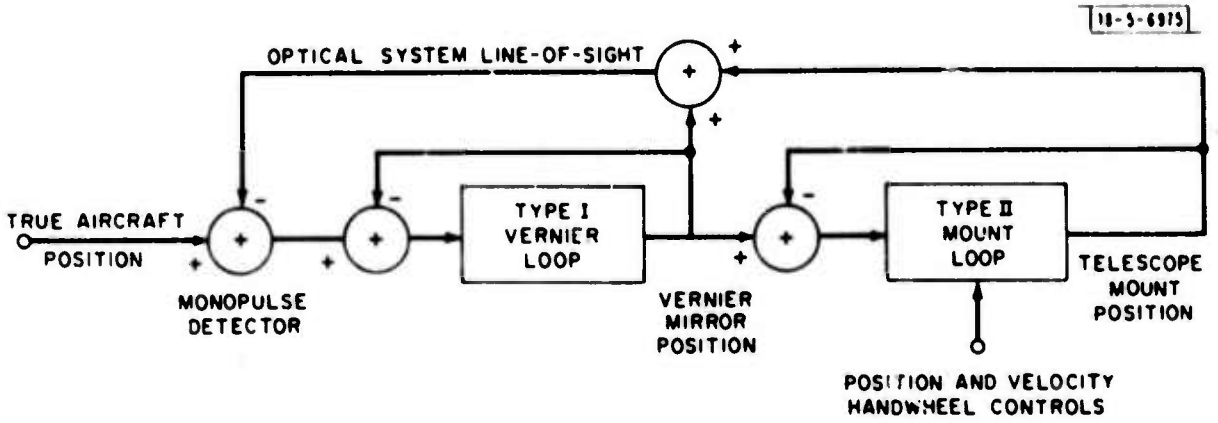

Fig. 9. Aircraft cascade tracking loop.

vernier mirror sees the target at its nominal boresight position. Acquisition in this configuration is somewhat non-trivial. The mount tracking loop is initialized by an operator by matching the filter velocity and position to that of the target. Then, when the IR returns are available, the monopulse signals start tracking the target with the vernier mirror and the main mount velocity and position prediction are carried out by the Type II tracking loop. Good tracking is maintained as long as the vernier offset command is within its field-of-view which is about ± 500 μrad. Since the mount tracking loop can have rather large errors (up to 500 μrad) while tracking the target, the mount tracking loop is purposely made slow to assure that the telescope motion is smooth and the two trackers do not "fight" each other. The 10/sec data rate is quite sufficient for this purpose.

III. EXPERIMENTS AND RESULTS

A. Error Curve Generation

Many tests and measurements have been necessary to perfect the monopulse system for satellite and aircraft tracking. The hardware performance has been assessed by the smoothness and symmetry of the system generated error curves (i.e., plots of error signals versus angle-of-arrival). Error curves were generated by scanning a test signal across the quad detector. Two methods were used - one "internal" and one "external." The internal test signal was generated by reflecting an attenuated transmit beam, before it reaches the telescope, back into the receiver optics. The attenuation is accomplished using CaF_2 windows of various thicknesses. The reflected transmit beam can be scanned across the detector by computer

commands to the transit time corrector shown in Figure 3. This internal method has the advantage that the system can be partially checked without going through the atmosphere as in external tests. Thus, variations in signal due to atmospheric turbulence and density variations are avoided. Internal tests do not give "real-world" results but are useful for alignment and preliminary checkout.

The external method of generating error curves was to slowly scan the transmit beam across a retroreflector positioned at the test tower 5.5 km away by means of the telescope vernier mirror. This signal could also be attenuated with CaF_2 to give weaker returns. Figure 10 shows error curves generated by the internal (in-house) and external (test tower) methods. Both curves were generated using the short range error processor. At the time, the gains of the azimuth and elevation channels had not been matched. The noisier test tower results are due to the aforementioned atmospheric effects. In fact, the test tower results were obtained under good "seeing" conditions when the atmosphere was relatively cooperative and uniform. Under bad "seeing" conditions, when the atmosphere is turbulent, error curves can hardly be distinguished.

Even if the atmosphere had no effect, one should not expect the two methods to yield identical error curves. In the internal method, a constant intensity beam scans the detector. In the external method, the return beam intensity from the corner cube varies since the focused incident beam with an Airy disk diameter of 10 cm scans a triangular retroreflector 3 cm on a side.

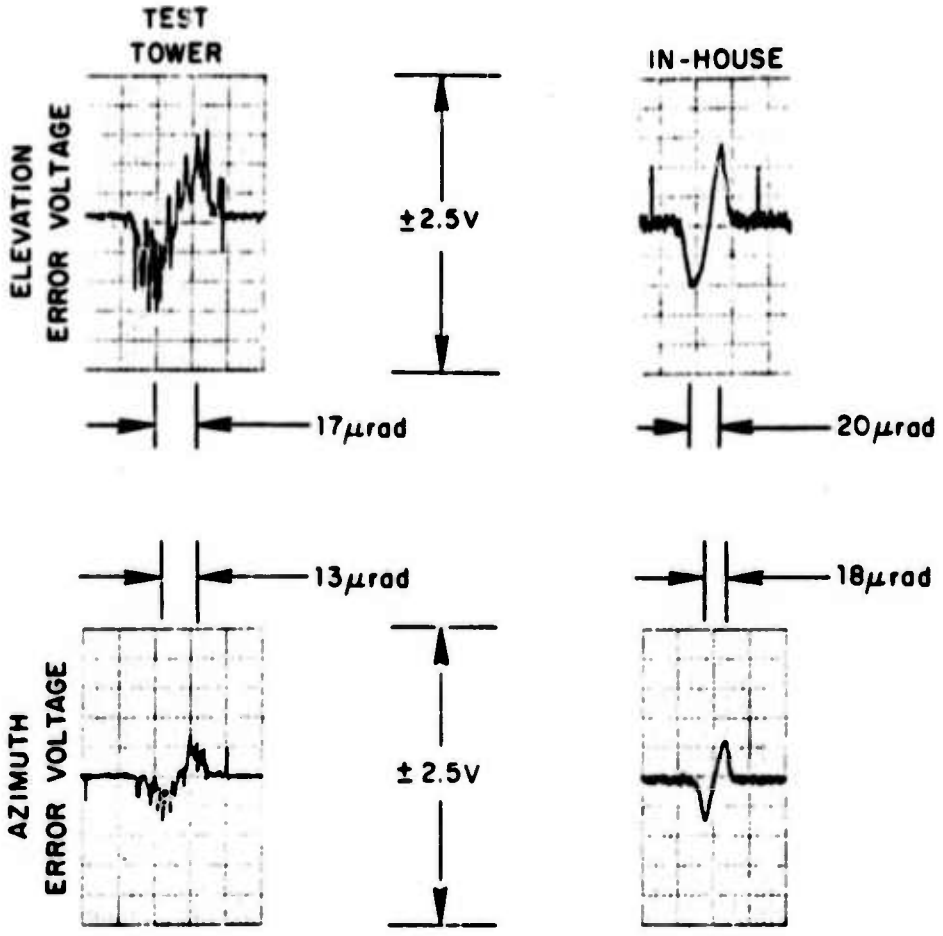

Fig. 10. Short-range processed monopulse error curves.

B. Test Tower Experiments

The first IR monopulse tracking experiments involved tracking the test tower retroreflector and recording angle-of-arrival statistics under different "seeing" conditions. During these experiments, the main telescope mount was held stationary, pointing at the test tower, while the tracking was accomplished by moving the vernier mirror. About 10μ watts of peak power was transmitted in the short range mode.

In Figure 11, the azimuth error, elevation error and the AGC voltage during good seeing conditions are shown as a function of time. In the tracking mode, during the first 1.7 minutes, the vernier mirror was allowed to track out the angle-of-arrival fluctuations. The resulting error curves appear smooth; the AGC voltage is consistently high. In the fixed pointing mode, when the vernier mirror was held stationary, the resulting error curves are noiser with angular fluctuations a large fraction of the 10 mrad beamwidth. The signal amplitude also fades for long periods of time.

Since the beam pointing system is quite stable and the test tower is expected to move very little; the different character of the signals of Figure 11 during tracking and pointing is believed to be caused almost exclusively by the atmospheric turbulence. Indeed, as the "seeing" gets worse, similar curves indicate an increase in the fluctuations.

To get an estimate of the statistical characteristics of the angle-of-arrival fluctuations, the test tower retroreflector was tracked as in the first half of Figure 11. The angle-of-arrival at any instant was estimated to be the vernier mirror position plus the monopulse error voltage. Figures 12 and 13 show the amplitude probability density functions and power

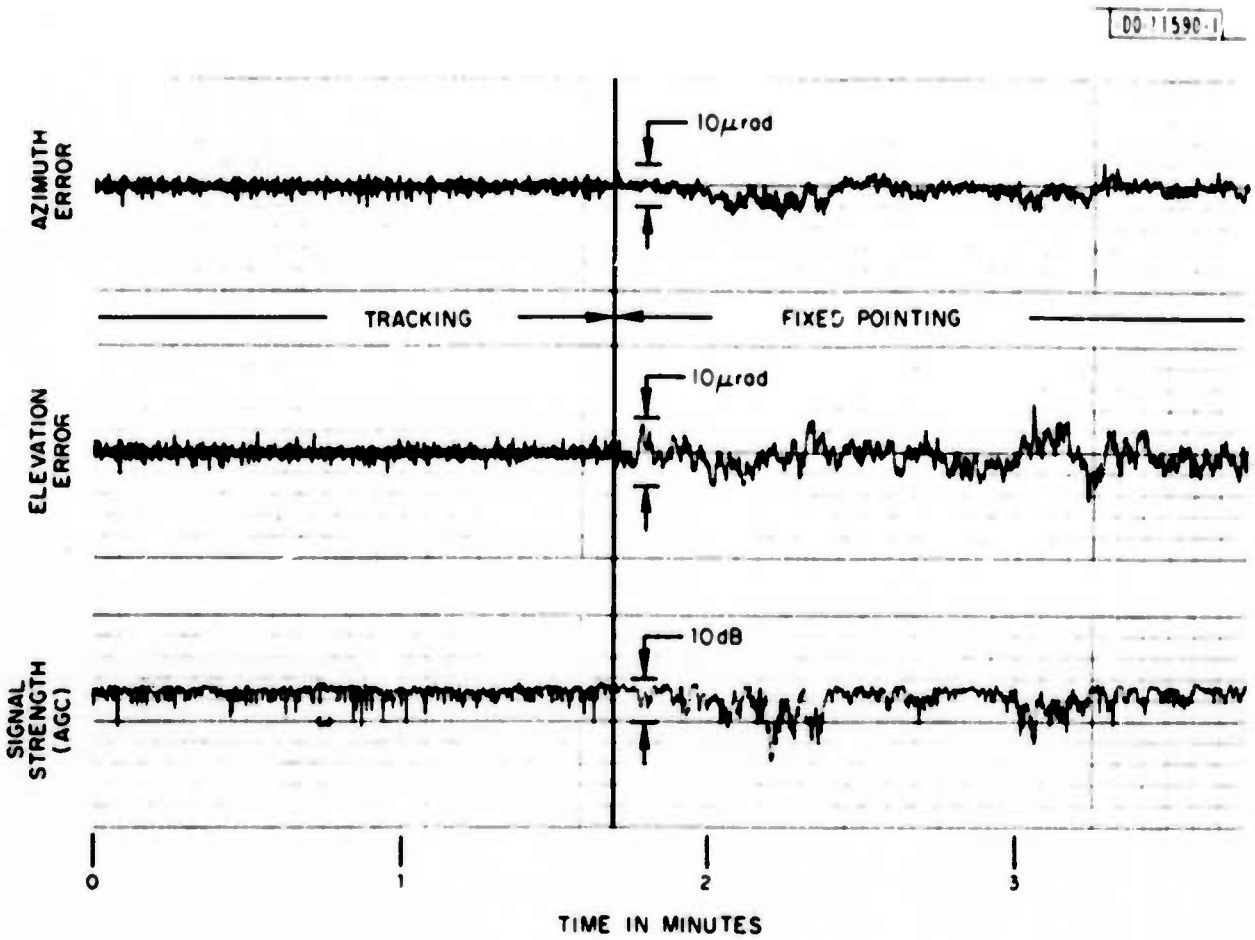

Fig. 11. Monopulse signals from retroreflector at a range of 5.5 km during good seeing conditions.

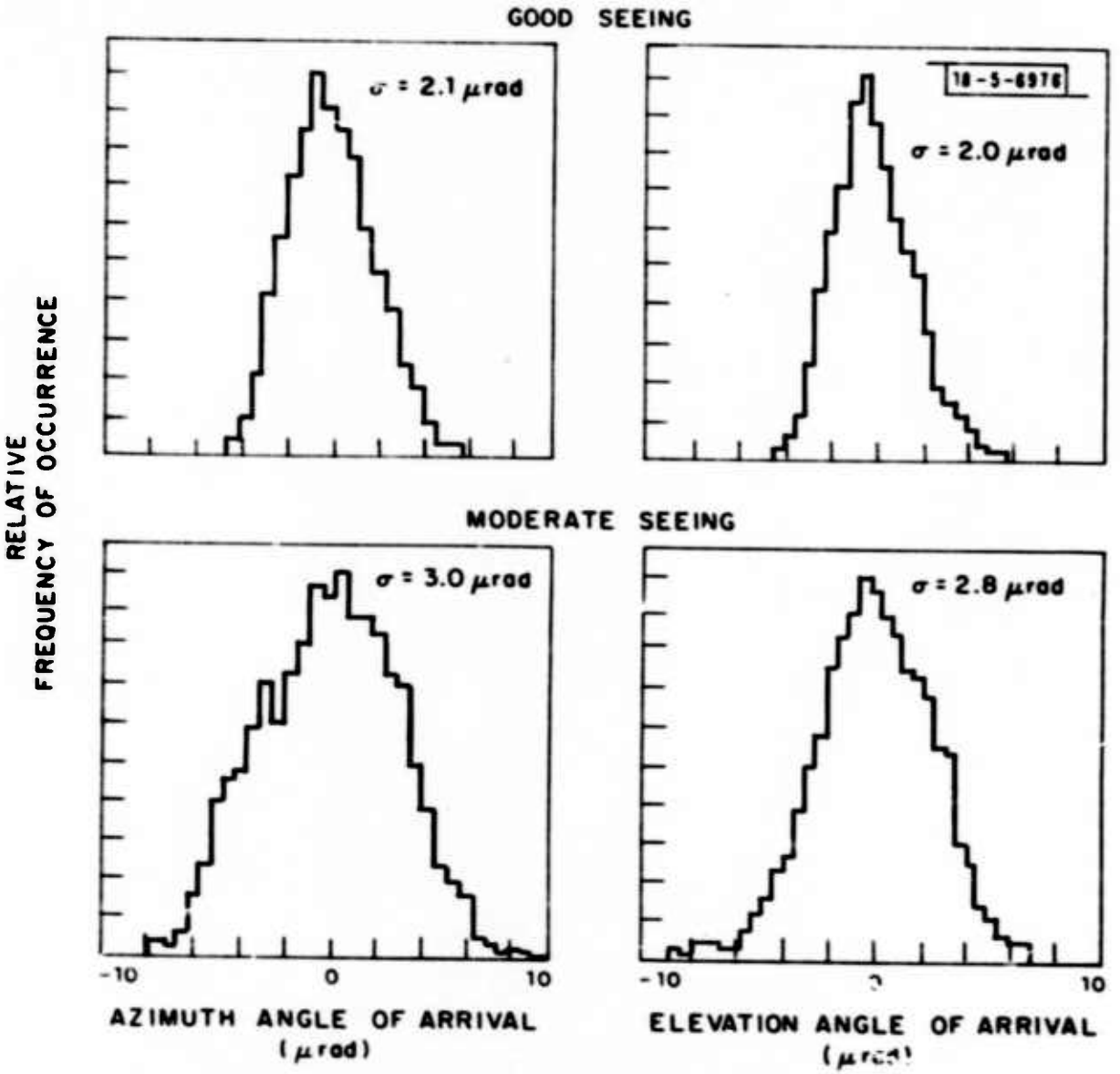

Fig. 12. Angle-of-arrival statistics during good and moderate seeing conditions for azimuth and elevation. Amplitude probability density function. Retroreflector target at a range of 5.5 km.

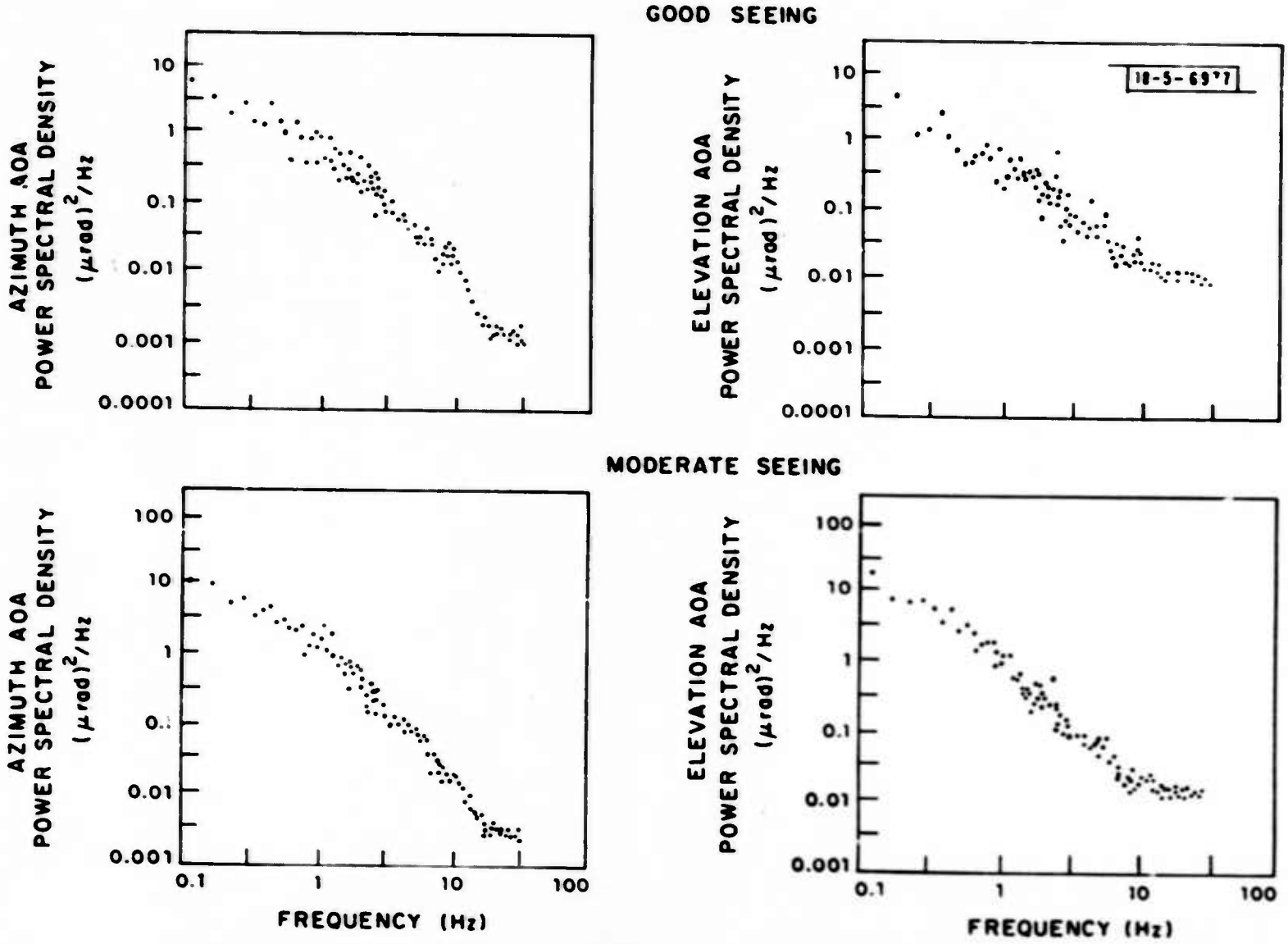

Fig. 13. Angle-of-arrival statistics during good and moderate seeing conditions for azimuth and elevation power spectral density functions. Retroreflector target at a range of 5.5 km.

spectral density functions obtained by estimating the atmospheric turbulence in this manner. The data were collected during good and moderate seeing as shown; however, the corner cube could not be tracked when poor seeing conditions were encountered since atmospheric turbulence caused beam deviations larger than a beamwidth.

These curves indicate typical measured results. At the time, the wind velocity and other atmospheric conditions along the 5.5 km path were not measured which would allow precise comparison to theoretically predicted statistics. The power spectral density shows a monotonically decreasing function with frequency. The frequency dependence is in general agreement with the predicted behavior[5] of $f^{-2/3}$ below the characteristic frequency and $f^{-8/3}$ above the characteristic frequency. The characteristic frequency is dependent on the aperture diameter and the cross wind as described by D. Greenwood.[5]

Figure 14 shows additional results of the tracking analysis. The vernier mirror position plus monopulse error indicates the total angle-of-arrival while the monopulse error by itself indicates the portion which the vernier mirror could not track out. Figure 14 shows that, when tracking, the standard deviation is reduced to 1 μrad (from 2 μrad) and the energy in the power spectrum below 2 Hz is greatly reduced. Similar improvements are obtained for azimuth during moderate seeing conditions; one example is shown by Figure 15. These curves show that the vernier mirror tracking loop is capable of tracking low frequency turbulence components up to 2 Hz.

These results confirm that for good to moderate seeing conditions, the existing monopulse tracker and the 2 Hz bandwidth vernier mirror can

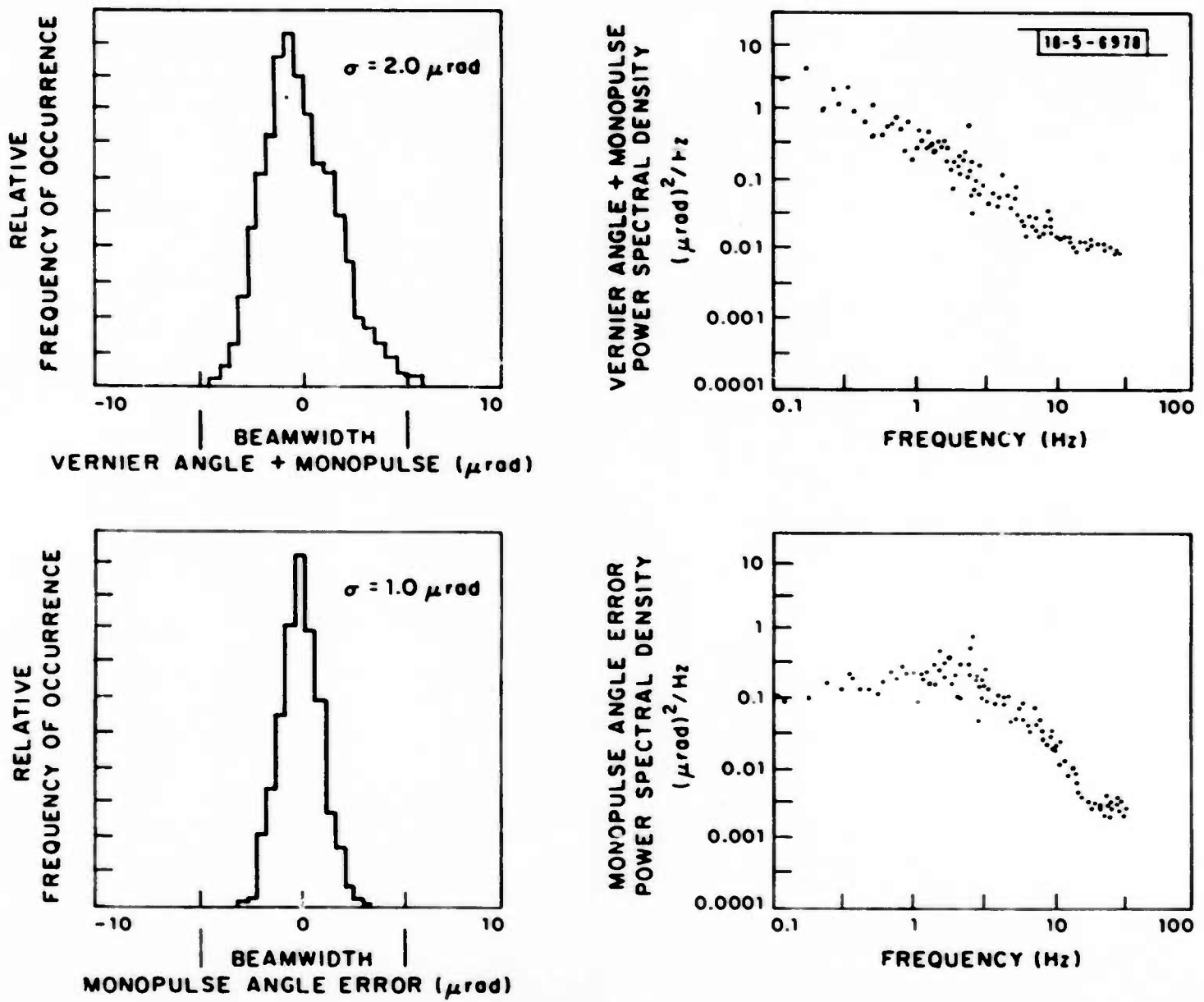

Fig. 14. Tracking data analysis in elevation only during good seeing conditions. Angle-of-arrival = residual monopulse error + vernier mirror position. Retroreflector target at range = 5.5 km.

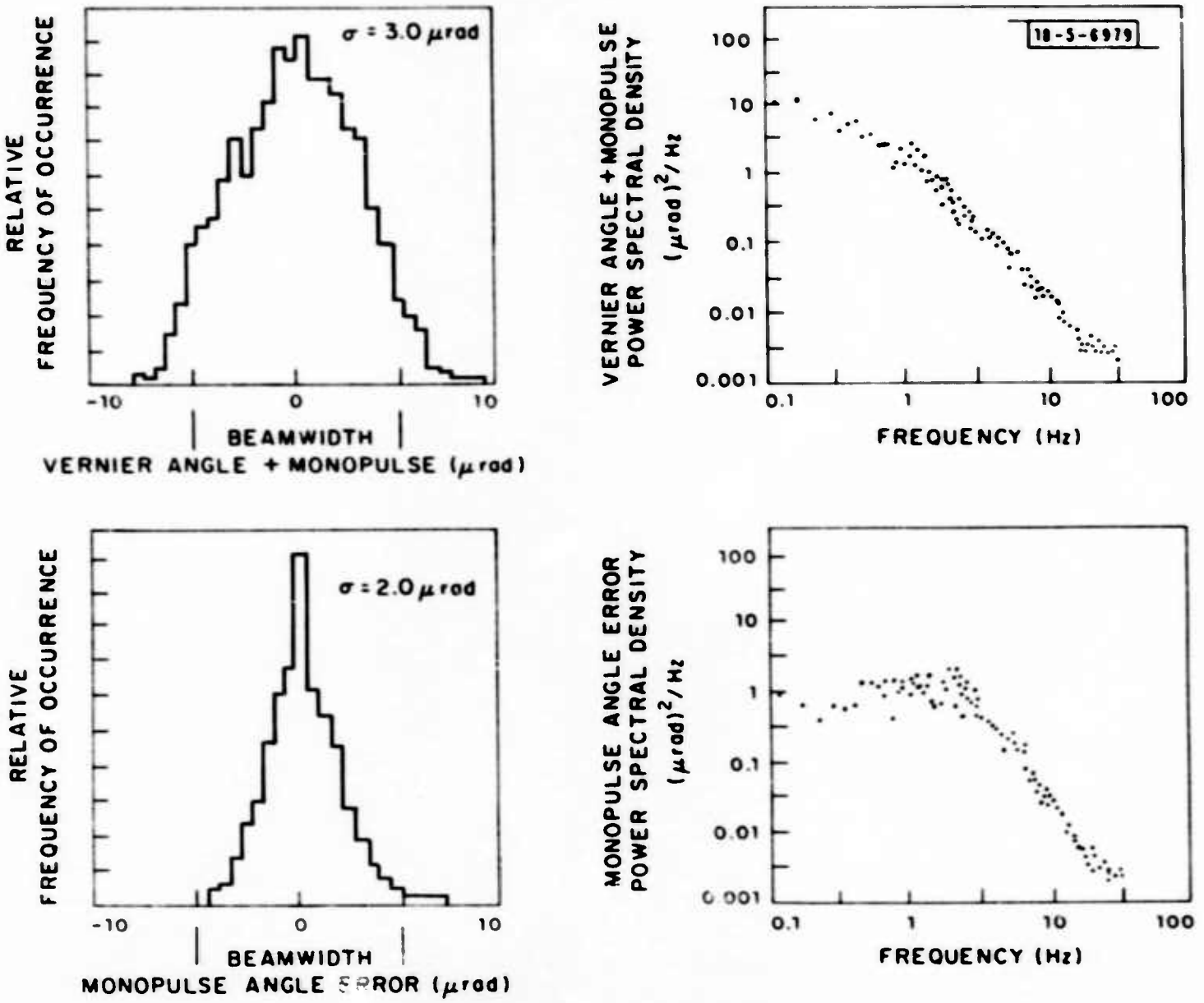

Fig. 15. Tracking data analysis in azimuth only during moderate seeing conditions. Retroreflector target at range = 5.5 km.

track out a measurable fraction of the angle-of-arrival fluctuations due to atmospheric turbulence. During poor seeing conditions, the amplitude of the high frequency components of the angle-of-arrival is greater than our 10 μrad beamwidth, which causes the tracker to lose the target. Since the path to the test tower is high above the valley floor (about 100 meters), the test tower angle-of-arrival fluctuations represent angle noise which might be typically encountered during an aircraft track.

C. Aircraft Tracking

The same vernier mirror tracking loop and the telescope tracker in the cascade mode, as shown in Figure 16, were used for tracking a retro-reflector on a cooperative aircraft. A visible TV image of the aircraft was used for acquiring the retroreflector, but once IR returns were received only IR monopulse signals were used for tracking. Again the short range processor was used.

Aircraft tracking experiments have been carried out on five or six occasions. Several system parameters have been varied to find most optimimum conditions for tracking. Typically, the aircraft was flown at 10-15 km range at a transmitter power in the 10-50 μwatt region. Tracking during good seeing and windless days, seems quite easy. During moderate seeing or gusty winds, the combination of atmospheric seeing and erratic aircraft motion makes tracking for more than a few seconds at a time impossible. With poor atmospheric conditions, it has been impossible to track at all.

The analysis of boresight visible TV recordings indicates that the tracks are reasonably smooth. When tracking is possible, visible image

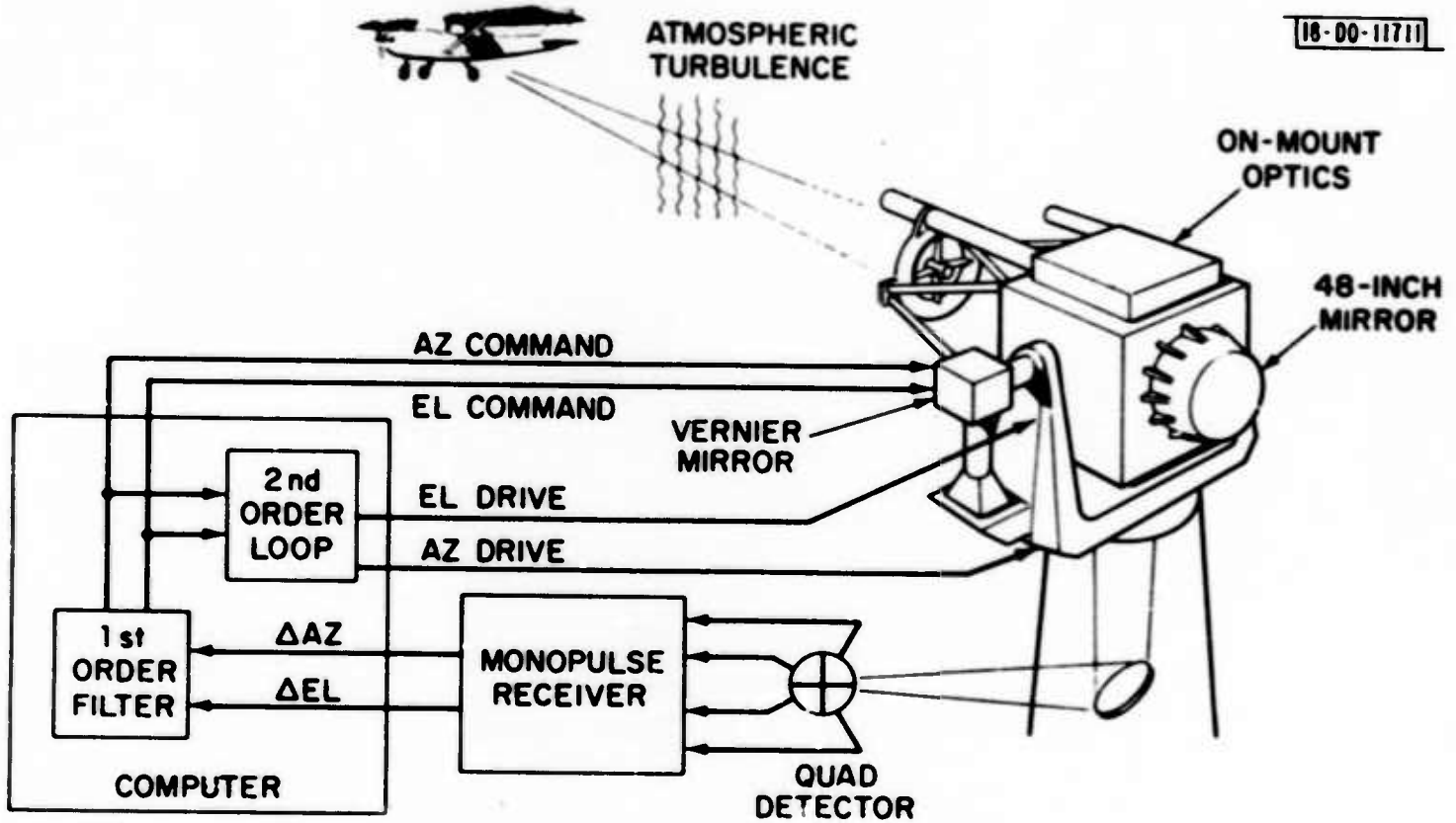

Fig. 16. Aircraft tracking mode of operation (short range mode).

jitter is in the order of 5-10 μrad. Because of the atmospheric angle-of-arrival fluctuations, jitter within a beamwdith has been expected to be large. The goal of the current experiments has been to investigate techniques of keeping the 10 μrad beam on the target for long periods of time rather than precise tracking within the beam.

D. Satellite Tracking

As indicated in Table 1, long range tracking of objects, such as satellites, involves different operating parameters. Since the range is longer, long pulses can be used and higher power is transmitted. In addition, the doppler frequency must be tracked or no IR returns are processed. The particular target on which long range monopulse tracking has been accomplished for the first time was a 3.8 cm diameter retroreflector installed for Lincoln Laboratory on the GEOS-III geodetic satellite. Figure 17 depicts the system mode used. The long range error processor after the monopulse receiver was used. The satellite was acquired with the aid of Millstone Hill Radar (MHR) adjacent to the Firepond facility and with the aid of visible tracking by the on-mount optics. While IR signals will be used in the Kalman filter in the future, presently crude pointing with better than 1 mrad accuracy is done with MHR information fed into a Kalman filter. Final IR tracking is accomplished via the vernier mirror servo system. The Kalman tracking with MHR provided the proper doppler freqeuncy designation so that IR returns could be detected by the receiver and the signal filter bank which displays the frequency power spectrum of the returns. As described earlier, a visible image obtained from solar illumination of the satellite is displayed

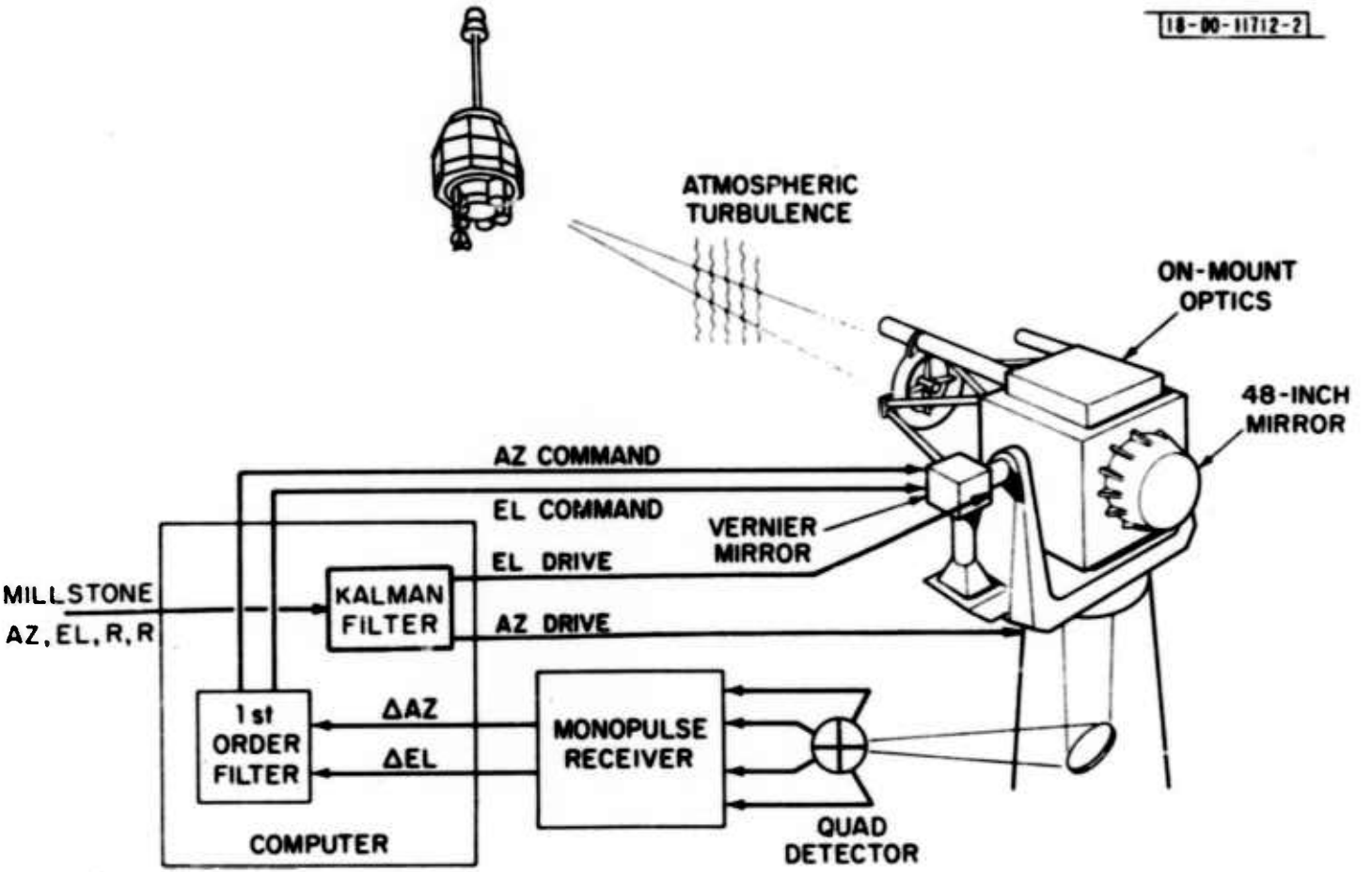

Fig. 17. Satellite tracking mode of operation (long range mode).

on the low light level TV (see Figure 3). IR tracking was attempted when IR "hits" were indicated in the filter bank display. Tracking parameters such as servo loop gains were adjusted until tracking occurred. 25 seconds of continuous "hands-off" tracking occurred while the satellite was at a range of 1100 to 1200 km, a doppler frequency range of 840 to 1000 MHz and a doppler rate of 6 MHz/sec. During the track, strong continuous returns with low residual monopulse errors were observed. The system PRF was 62.5 Hz, pulse length 4 msec, and the transmitted peak power was 400 W.

Figure 18 shows elevation angle tracking statistics, during 20 seconds of completely automatic track. The vernier mirror statistics now describe the difference between the Kalman filter generated pointing data and the monopulse determined line-of-sight. The histogram of the vernier mirror angle added to the monopulse error, indicates that the coarse pointing errors changed by almost 100 μrad during the twenty second period which the vernier had to track. The monopulse angle error histogram shows that during this time the RMS tracking error was only 1 μrad.

The comparison of power spectral density functions shows that the tracker bandwidth is about 1 Hz. This is slightly narrower than the bandwidth obtained during Test Tower or Aircraft tracking in the short range mode. Since the servo gains were adjusted in real time, just before this section of track, they may have been slightly lower than optimum for the track. However, the additional delays due to the 1000 km range and the lower sampling rate of 31.25/sec which is caused by the 62.5 Hz PRF and monopulse error signal data processor may not have allowed a higher loop gain.

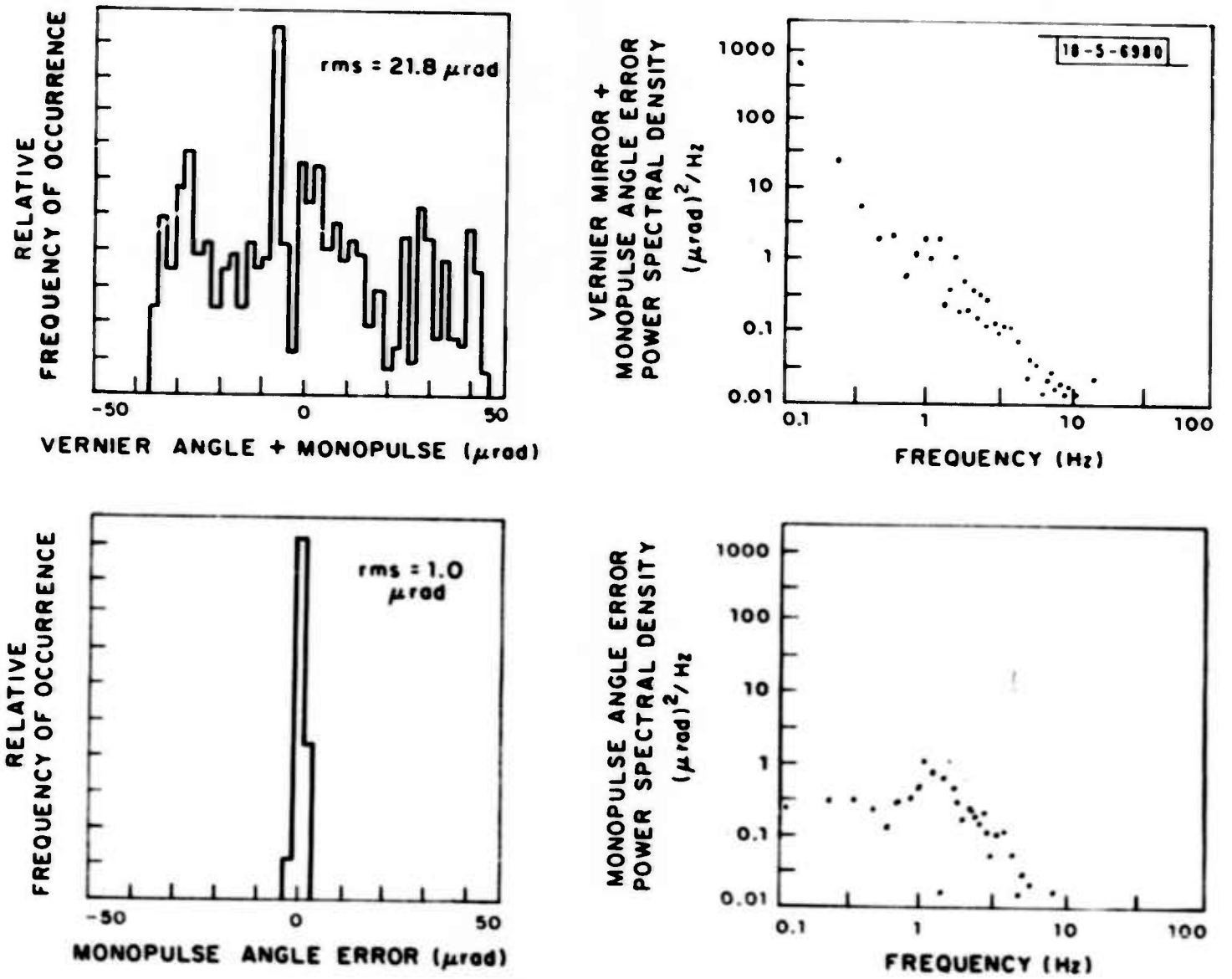

Fig. 18. Tracking data analysis in elevation only of monopulse errors from GEOS-III retroreflector at range of about 1100 km.

IV. SUMMARY

10.6 μm coherent monopulse tracking of retroreflectors has been accomplished on cooperative aircraft and the GEOS-III satellite, and the angle-of-arrival statistics on the Test Tower retroreflector during reasonable seeing conditions have been determined. Although the initial results are highly successful, the reader should be cautioned that the experiments are really technique demonstrations using existing non-optimized hardware. Improvement in tracking loop characteristics will be needed, for example, to shorten the response time so that tracking can be accomplished during poor seeing conditions.

ACKNOWLEDGMENTS

The authors wish to express their appreciation to the many members of the Firepond staff and Group 54 who assisted in different aspects of the experiments described in this report and made the results possible.

REFERENCES

1. R. J. Keyes and T. M. Quist, "Low-Level Coherent and Incoherent Detection in the Infrared," in Semiconductors and Semimetals, Vol. 5 (Academic Press, New York, 1970), pp. 321-359.

2. M. C. Teich, "Coherent Detection in the Infrared," in Semiconductors and Semimetals, Vol. 5 (Academic Press, New York, 1970), pp. 361-407.

3. D. L. Spears, "Planar HgCdTe Quadrantal Heterodyne Arrays with GHz Response at 10.6 μm," to be published in Infrared Physics.

4. R. G. Brown, Smoothing, Forecasting and Prediction of Discrete Time Series (Prentice-Hall, Englewood Cliffs, New Jersey, 1963).

5. D. P. Greenwood and D. L. Fried, J. Opt. Soc. Am. 66, 193-206 (1976).